



Utilizing the Sentinel-6 Michael Freilich Equivalent Number of Looks for Sea State Applications

Lisa Recchia ^{1,†}, Pietro Guccione ^{1,*,†} , Thomas Moreau ^{2,†} and Craig Donlon ³

¹ Aresys, 20132 Milan, Italy; lisa.recchia@aresys.it

² CLS, 31000 Toulouse, France; tmoreau@groupcls.com

³ European Space Research and Technology Centre (ESTEC), European Space Agency (ESA), 2201 BL Noordwijk, The Netherlands; craig.donlon@esa.int

* Correspondence: pietro.guccione@aresys.it

† These authors contributed equally to this work.

Abstract: Sentinel-6 Michael Freilich (S6-MF) is the first altimeter operating in a continuous high-rate pulse mode, i.e., interleaved mode. This ensures the generation of low-resolution (LR) mode measurements with a pulse repetition frequency (PRF) of ~ 9 kHz (variable along the orbit) for the Ku-band as well as the processing of high-resolution (HR) echoes on ground. This operating mode provides an elevated number of highly correlated single looks with respect to the fewer number, weakly correlated echoes of Jason-3 altimeter. A theoretical model is exploited to envisage the correlation properties of S6-MF pulse limited waveform echoes for different sea-state conditions; after that, the model is validated by comparison with the equivalent number of looks (ENL) empirically estimated from real data. The existence of a significant dependence of the statistical properties on the range is verified, and its impact on the precision and on the accuracy in the estimation of the geophysical parameters is assessed in case of the 9 kHz PRF of S6-MF. By applying pulse decimation before the multilook processing, an investigation on new processing techniques is performed, aimed at exploiting the higher ENL in S6-MF low-resolution mode waveforms. It is shown that a bias of less than 0.4 cm is found for SSH and about 1.5 cm for SWH at SWH = 2 m when the decimated waveforms processing is compared with full high-PRF processing.

Keywords: Sentinel-6; Jason-3; delay-doppler altimeter; sea-state; geophysical parameters



Citation: Recchia, L.; Guccione, P.; Moreau, T.; Donlon, C. Utilizing the Sentinel-6 Michael Freilich Equivalent Number of Looks for Sea State Applications. *Remote Sens.* **2024**, *16*, 1866. <https://doi.org/10.3390/rs16111866>

Academic Editor: Ali Khenchaf

Received: 3 April 2024

Revised: 16 May 2024

Accepted: 21 May 2024

Published: 23 May 2024



Copyright: © 2024 by the authors. Licensee MDPI, Basel, Switzerland. This article is an open access article distributed under the terms and conditions of the Creative Commons Attribution (CC BY) license (<https://creativecommons.org/licenses/by/4.0/>).

1. Introduction

Altimetry satellites play a crucial role in monitoring and understanding various aspects of the Earth's oceans, including sea state. These satellites utilize advanced radar systems to measure the height of the sea surface with remarkable precision, offering valuable insights into ocean dynamics and phenomena. By emitting microwave pulses towards the Earth's surface and recording the time taken for the signals to return, altimetry can accurately determine sea surface height variations. These data enable scientists to assess parameters such as wave height, wind speed, and ocean currents, providing vital information for weather forecasting, climate research, and maritime operations [1]. Through continuous monitoring and analysis, altimetry satellites contribute significantly to our understanding of oceanic processes and their impact on global climate systems.

The radar altimetry measures the two-way travel time of a radar pulse between the satellite antenna and the Earth's surface at the nadir of the spacecraft. This measurement is performed through the collection of the waveforms bounced back by the reflecting facets within the altimeter footprint. While the traditional pulse-limited radar altimeters were used to collect information on the sea level and slope [2], the delay-Doppler concept [3], thanks to the higher along-track resolution, has been used to obtain information of the shape, balance velocities and contribution to sea level in open waters, large ice sheets [4,5], marine ice thickness [6], or lake ice [7].

Radar echoes are intrinsically affected by speckle noise, due to coherent summation of many randomly phased scatterers from the surface [8]. Multilooking, i.e., incoherent averaging of single look echoes, is performed in order to achieve a speckle reduction. Delay/Doppler (DD) altimetry has shown to be more effective in reducing the speckle since a higher number of looks than in the conventional radar altimeter is gained. This is due also to the high number of the individual waveforms in each Doppler bin that is, for Delay/Doppler altimeters, equal to the number of pulses in a burst [9].

However, due to the correlation among the averaged single looks, the effective number of looks (ENL) is reduced. By definition, the ENL is the number of independent observations that are obtained by the radar from a distributed target per unit of time. The ENL can be achieved by multilooking a fixed number of echoes, thus impacting the statistical properties of the final multilooked waveform. The ENL is then a figure to quantify the speckle suppression obtained by multilooking in radar signals.

A seminal study to determine the correlation properties of consecutive pulses from nadir-looking pulse-limited radar altimeters is [10]. The study provides a value for the maximum pulse repetition frequency for which the statistical independence of consecutive waveforms is still assured. Since the TOPEX/Poseidon Mission launched in 1992, up to the Jason altimeter series, conventional low-resolution mode (LRM) altimeters were designed to obtain uncorrelated echoes. The reason was to have efficient satellite operations in terms of power usage, at the same time maximizing the information achieved from the transmitted pulses. Following these design criteria, the pulse repetition frequency (PRF) for the Jason series was selected to be approximately 2 kHz.

Copernicus Sentinel-6 Michael Freilich is the first altimeter operating in a continuous high-rate pulse mode. This design allows the simultaneous production of low-resolution mode measurements with a pulse repetition frequency of ~ 9 KHz for the Ku-band as well as the processing of high-resolution echoes on ground. S6-MF thus generates an elevated number of highly correlated single looks, with respect to the fewer number of Jason-3 uncorrelated pulses.

In the theoretical model shown in [11], for the LRM waveforms, the average of a high number of correlated single looks (~ 9 KHz) provides a higher ENL with respect to the case in which fewer and almost uncorrelated single looks are averaged. From this analysis, a stronger dependence with respect to the low-PRF case of the ENL on the range gate of the multilooked waveforms emerged. This dependence was later confirmed from successive analysis performed on an extensive dataset of 5 years pseudo-LRM Cryosat-2 data taken over ocean [12] or, more recently on high-resolution Sentinel-6 data analysis [13]. This last work showed that, despite the fact that at higher PRFs the noise in the estimation of geophysical parameters is reduced, the significant dependence of the statistical properties on the range gate introduces significant biases in the retracked parameters using least-square estimation approach. These biases have been found to be dependent on the sea geophysical parameters and need to be properly accounted for, to ensure seamless continuity of sea level monitoring between S6-MF and Jason-3, the new and previous reference missions of the ocean surface topography satellite series.

More recently [14], the autocorrelation properties of Sentinel-3A SAR mode waveforms over open ocean have been studied to assess the effect on the retrieval of ocean geophysical parameters at various posting rates. This study confirmed the strong dependence of the decorrelation length with the multilooked SAR mode waveforms. A similar analysis [15], based on a theoretical model, showed the power correlation variability with respect to the waveform range gate in case of SAR mode single-look waveforms. The outcome of these studies highlights that, at high PRF, the significant variability in the statistical properties of the range gates in typical L1b 20-Hz multilooked waveforms must be properly addressed when integrating Sentinel-6/Jason-CS data in a climatological data record.

In this paper, we consolidate the correlation properties of the LR-mode waveforms as a function of the sea wave height by comparing the theoretical model in [15] with ocean data from recent S6-MF acquisitions. The accuracy and the precision of the geophysical

parameters estimated from open ocean are shown as bias of the estimation evaluated with different decimation factors with respect to the evaluation at full PRF. Finally, the behavior of the ENL in case of higher posting rate is discussed.

2. Pulse-To-Pulse Correlation Model and ENL

The evaluation of the single look correlation is described in [15] and is here shortly summarized.

The echoes acquired by a radar altimeter are affected by speckle and the purpose of multilooking is to reduce the fluctuations due to speckle. Let Ψ denote an individual echo and $p = \Psi\Psi^*$ the echo power obtained by multiplication of an echo signal with its complex conjugate. Since individual echoes have real and imaginary parts that are zero-mean Gaussian distributed (echoes come from backscattering of many facets, so central limit theorem applies), their power p is exponentially distributed and, consequently, its variance is equal to the square of its mean \bar{p}^2 .

A multilooked echo q is achieved by averaging N independent echo powers:

$$q = \frac{1}{N} \sum_{n=0}^{N-1} p_n \quad (1)$$

The variance of the multilooked signal is

$$\sigma_q^2 = \frac{\bar{p}^2}{N} \quad (2)$$

from which N can be retrieved:

$$N = \frac{\bar{p}^2}{\sigma_q^2} \quad (3)$$

This result exactly holds for independent identically distributed (i.i.d.) power echoes. In general, due to single-look correlation and mean-power differences of the averaged waveforms, the variance of multilooked products is larger than expected.

The effective number of looks (ENL) is defined as the estimate of the effective number of statistically independent looks for the backscattered power and is upper bounded by the actual number of single look echo waveforms averaged together. The higher the ENL, the more efficient the speckle noise mitigation and, therefore, the lower the error in the final estimation of geophysical parameters.

Thus, the ENL can be computed as follows:

$$ENL = \frac{|\bar{q}|^2}{\sigma_q^2} \quad (4)$$

After some calculation, it can be shown that

$$ENL = \frac{\bar{q}\bar{q}^*}{\sigma_q^2} = \frac{\left| \sum_{n=0}^{N-1} \hat{p}_n \right|^2}{\sum_{n=0}^{N-1} \sum_{m=0}^{N-1} \bar{p}_n \bar{p}_m R_{n,m}} \quad (5)$$

where $R_{n,m}$ denotes the correlation coefficients (also called coherence) of the power echoes p_n and p_m . In case of low-resolution mode, the pulse-limited echoes summed together in a multilook echo can be assumed drawn from the same mean, thus leading to a simplified expression for Equation (5):

$$ENL = \frac{\bar{q}\bar{q}^*}{\sigma_q^2} = \frac{\left| \sum_{n=0}^{N-1} \hat{p}_n \right|^2}{\sum_{n=0}^{N-1} \sum_{m=0}^{N-1} \bar{p}_n \bar{p}_m R_{n,m}} = \frac{N^2}{\sum_{n=1}^{N-1} \sum_{m=1}^{N-1} R_{n,m}} \quad (6)$$

The previous assumption is reasonable if geophysical parameters are slowly variant in space and in the extent of a radar cycle.

The power echoes coherence as a function of the delay τ can be computed by evaluating the correlation between two identical echoes, observed with a small along-track displacement x :

$$R(\tau, x) = \frac{\overline{\Psi(\tau)\Psi(\tau, x)^*}}{\overline{\Psi(\tau)\Psi(\tau)^*}} = \left| \frac{C(\tau, x)}{p_r(\tau)} \right| = \left| \frac{p_t(\tau) * p_z(\tau) * \Pi(\tau, x)}{p_t(\tau) * p_z(\tau) * X(\tau)} \right| \quad (7)$$

At the denominator of Equation (7), we have the mean echo power obtained by the triple convolution of the point-target impulse response $p_t(\tau)$, the sea-surface height probability density function $p_z(\tau)$, which accounts for the dependence on the significant wave height (SWH), and the surface impulse response $X(\tau)$, defined in [16]. At the numerator of the equation, we have the covariance $C(\tau, x)$, which is given again by a triple convolution but instead of the surface impulse response there is the covariance impulse response $\Pi(\tau, x)$ given by [4]:

$$\Pi(\tau, x) = \frac{\lambda^2 G_0^2 c \sigma_0}{32\pi^2 h^3 \eta} H\left(\tau + \frac{\eta h}{c}\right) \int_0^{2\pi} \exp\left\{2ik_0 x \sqrt{\frac{c\tau}{h\eta}} \cos\vartheta\right\} \exp\left\{-2\frac{c\tau}{h\eta} \left(\frac{\cos^2\vartheta}{\gamma_1^2} + \frac{\sin^2\vartheta}{\gamma_2^2}\right)\right\} d\vartheta \quad (8)$$

where λ is the carrier wavelength, G_0 the antenna gain, c the light speed, σ_0 the ocean backscattering coefficient, h is the satellite altitude, and $\eta = 1 + h/R$ with R being the Earth radius is a geometric correction factor for the spherical surface. H is the Heaviside step function and the last term is a circular integration along an isorange line, with k_0 being the carrier wavenumber and γ_1 and γ_2 the antenna illumination width in the along- and across-track directions.

As can be seen from Equation (7), the power correlation is a function of both the delay time τ and the along track distance x at which the echoes are placed, and depends on the SWH as a consequence of the convolution with the sea-surface height probability density function p_z . Starting from Equation (7), the power correlation can be computed using numerical integration for different delay times τ and different along track displacements x , accounting for that the actual satellite displacement in along track direction between each pair of pulses depends on PRF and satellite velocity.

3. Power Correlation Analysis

In the following, the pulse-to-pulse autocorrelation as a function of the delay time and along-track displacement is shown for different S6-MF real datasets acquired over open ocean and in different sea conditions. In detail, different SWH are considered.

Figure 1 shows the pulse-to-pulse autocorrelation $R(\tau, x)$ as a function of the delay time τ and the along-track displacement x computed for S6-MF LR mode echoes for two different ocean states: $SWH = 2$ m (Figure 1a) and $SWH = 8$ m (Figure 1b).

It is worth remembering that the values of R are represented only for positive values of along-track displacement because the autocorrelation is symmetric with x .

As expected, the pulse-to-pulse autocorrelation is identically 1 for $x = 0$ (i.e., an echo is perfectly correlated with itself), while its value decreases at the increase of x (vertical axis), i.e., echoes acquired at larger along-track distances are less and less correlated each other. The autocorrelation achieved using S6-MF data is in agreement with the autocorrelation found for Cryosat data and is shown in Figure 2a of [12].

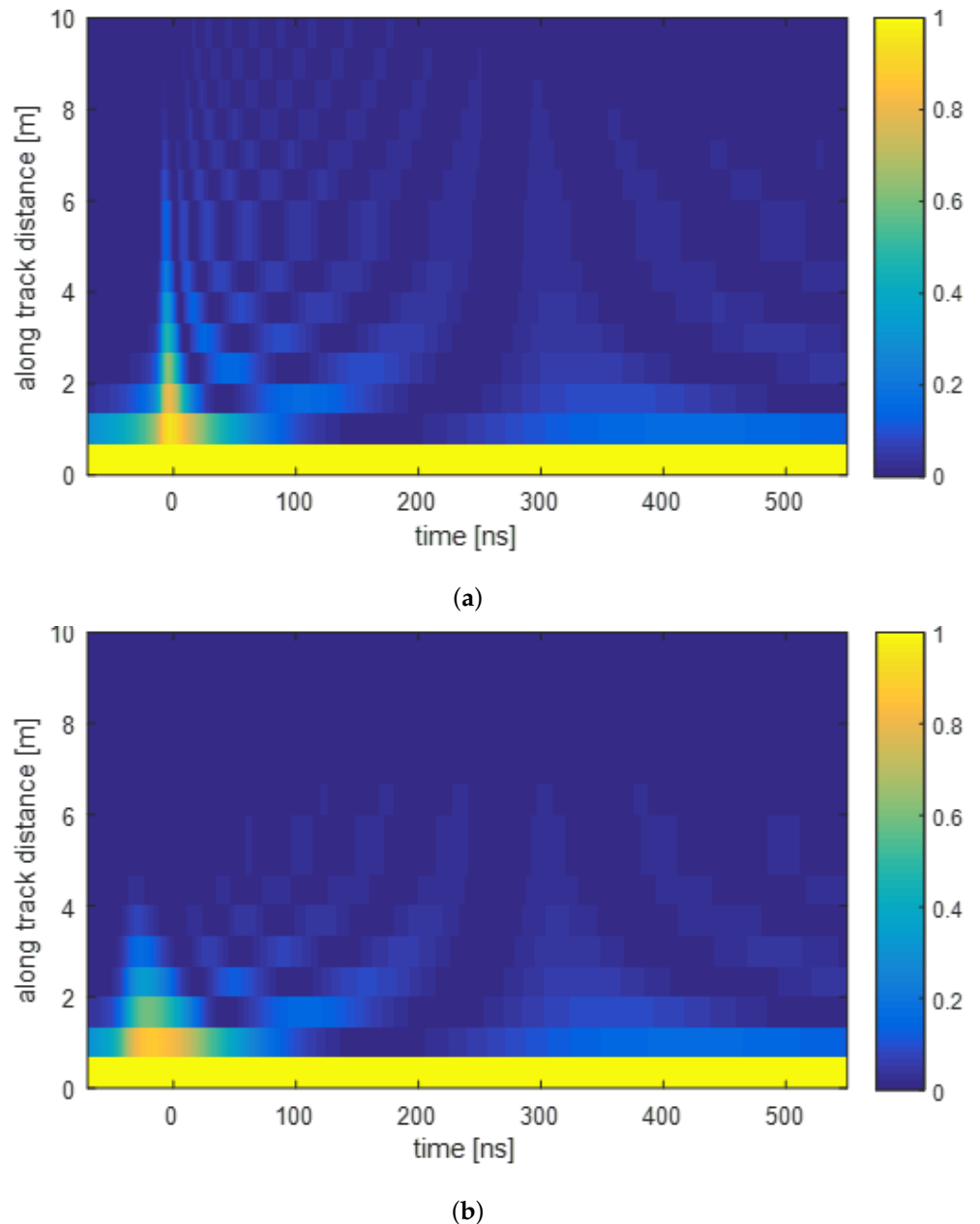


Figure 1. Pulse-to-pulse autocorrelation function, $R(\tau, x)$, as a function of the delay time τ and the along-track displacement x for S6-MF LR mode echoes and two different ocean states with $SWH = 2$ m (a) and $SWH = 8$ m (b).

Additionally, in the relatively calm ocean state (with a moderate value of $SWH = 2$ m Figure 1a), the decay of the correlation with the along-track distance is slower than in case of a rougher ocean state with a quite large $SWH = 8$ m (Figure 1b).

The time axis in Figure 1 refers to the relative pulse delay with respect to the surface (delay $\tau = 0$ s). Negative delays then correspond to the instants preceding the arrival of the radar return, while positive delays are associated with the waveform trailing edge. For comparison, Figure 2b reports the pulse-limited power waveforms obtained from the waveform model and for different SWH values on the same delay axis.

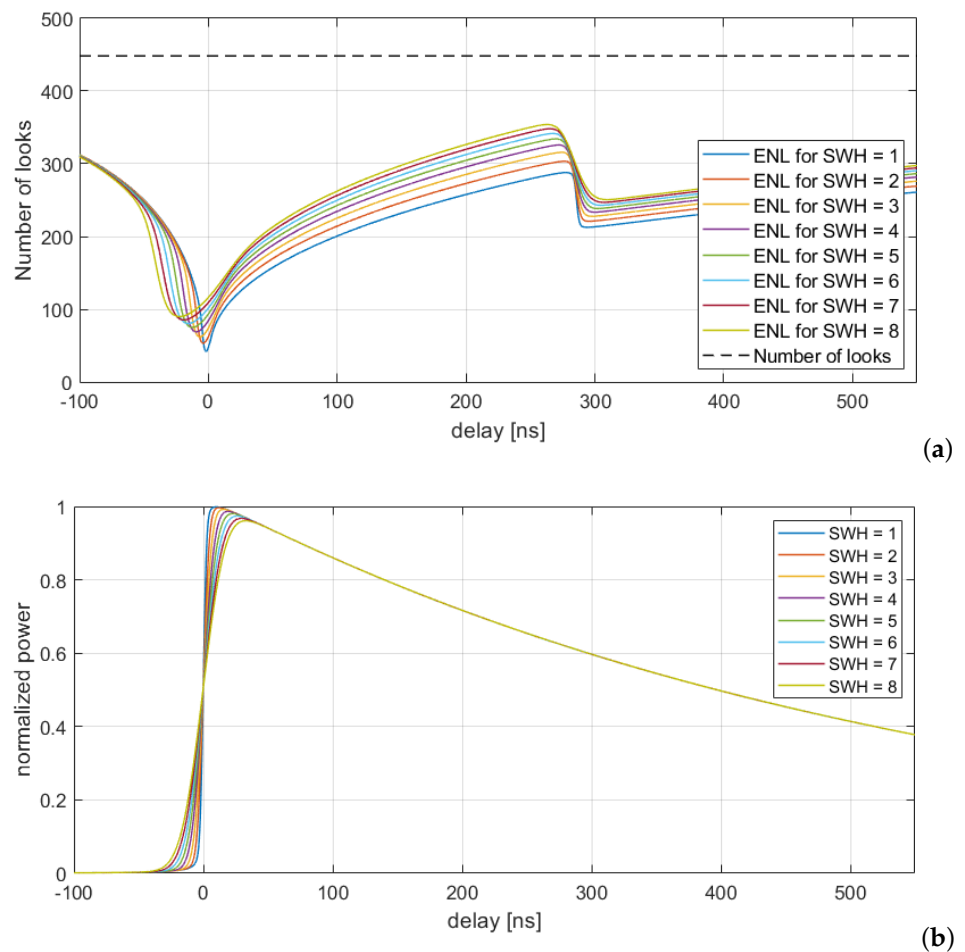


Figure 2. (a) Theoretical ENL (solid-line) as a function of the delay time τ for S6-MF LR mode echoes obtained by averaging all the available pulses in a tracking cycle for different sea SWH. For comparison, the number of averaged echoes is plotted as a dashed line. (b) Pulse-limited power waveform for the same sea SWH.

4. ENL Analysis

4.1. Theoretical ENL and Power Waveform

The power correlation function R allows the evaluation of the theoretical ENL according to Equation (6). To this aim, the along-track distance of each pair of pulses to be included in the multilooking are selected according to the instrument chronogram, i.e., the displacement in the along-track direction of the satellite between each pair of pulses is computed according to the PRF and satellite velocity. The assumption is to have a homogeneous wave height condition in the extent of the multilooking time.

Figure 2a shows the theoretical ENL for different wave heights for S6-MF LR mode echoes, obtained by averaging all the available pulses in a tracking cycle. For comparison, the number of averaged echoes, representing the upper bound for the ENL, is plotted as a dashed line on the top. This ENL value would be obtained only in the case of complete decorrelation of the averaged echoes.

Figure 2b shows the pulse-limited power waveforms obtained with S6-MF parameters and the same range of SWH values. This plot provides a correspondence between the ENL trend and the power waveforms trend in the different areas: the thermal noise area, the leading edge, and the trailing edge.

As can be seen from Figure 2a, an increasing SWH produces an overall enhancement of the ENL, due to the progressive decorrelation of the averaged pulses. Moreover, for all the SWH values, the resulting ENL shows an extremely variable dynamics along the delay

time dimension, with the lowest value achieved at the leading edge and higher values obtained at the waveform trailing edge.

As expected, the continuous high-rate pulse mode of S6-MF provides an elevated number of highly correlated single looks, which translates to a ENL much smaller than the actual number of averaged values. This is also confirmed by the results in Figure 2a.

4.2. Theoretical and Data-Based ENL in Subsampled Multilook

Considering the decrease in the pulse-to-pulse correlation for larger values of along-track distances, an alternative multilooking method is considered, consisting of averaging a lower number of waveforms by an integer decimation, so as to reduce the correlation among successive waveforms. Different decimation factor can be used.

Figure 3 shows the theoretical ENL (solid lines) obtained from different incoherent averaging decimation strategies and for two different values of SWH. Two decimation strategies were used:

- Taking one pulse out of two, leading to an equivalent acquisition frequency of ~ 4.5 KHz;
- Taking one pulse out of five, leading to an equivalent acquisition frequency of ~ 1.8 KHz close to the Walsh limit.

As expected, for the considered multilooking methods, the ENL is lower than the one obtained for the 9 KHz case, but it is much closer to the actual number of averaged echoes, addressed by the dashed line of the corresponding color.

As limit, for the 1.8 KHz case, the ENL is almost coincident with the number of averaged echoes, as expected from the decorrelation of the single-look pulses. Moreover, the ENL in correspondence of the leading edge (i.e., delays close to 0) is very similar for all three cases, while the greatest differences are observed in the trailing edge region.

The theoretical plots were replicated using true data from S6-MF cycle 9 data over open ocean. L1A were bprocessed with different decimation factors, and a retracker based on the model in [15] was applied to estimate the SWH values. Finally, portions of data with omogeneous SWH values were used to obtain an empirical estimation of the ENL for different sea wave heights. In Figure 4, the ENL is shown for different values of SWH and (1, 2, 5) as decimation factors. The corresponding dashed lines represent the averaged number of echoes.

The ENL retrieved from data are in line with the theoretical result, although some points need to be discussed.

First, the different behavior of the leading edge at various SWH (see Figure 2b) is explained by the increasing of azimuthal dispersion, which generates a larger bandwidth. This produces a faster pulse-to-pulse decorrelation and the blunter shape of the leading edge waveform. Part of the energy of the leading edge, then, leaks into the noise area.

For the noise area, in both theoretical and data-based plots, it would be expected that ENL in the noise area were equal to the number of looks averaged (see Figures 3 and 4) due to the decorrelation introduced by the thermal noise. Instead, an asymptotic trend towards such value is seen. This behavior is just due to the leakage of the leading edge energy mentioned before. Due to this leakage, the waveform results partially correlated also in the noise area, at least in proximity of the leading edge. As SWH increases, due to the blunter leading edge shape, the asymptotic value (i.e., the theoretical ENL) is reached slower. Moreover, since the theoretical curves, as in Figure 3, do not include the noise, the real number of looks in the noise area is higher (due to the presence of the noise, that decorrelates), as can be seen when comparing the solid and dotted lines in Figure 4.

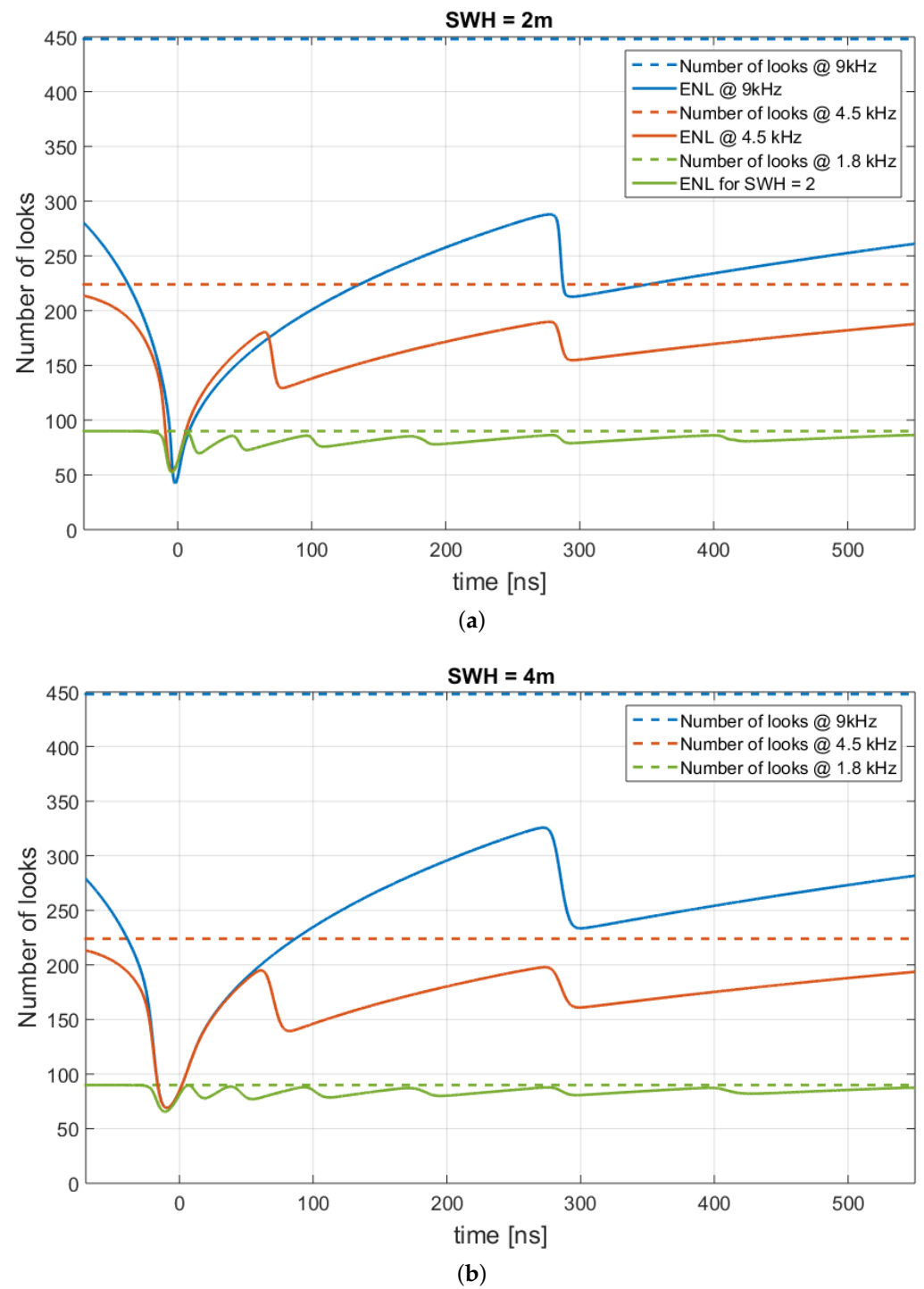


Figure 3. Theoretical ENL values for two values of SWH. Theoretical ENL (solid-line in a and b) is plotted as a function of the delay time τ and different decimation factors; the corresponding number of averaged echoes are in dashed lines and the same color. (a) $SWH = 2$ m; (b) $SWH = 4$ m.

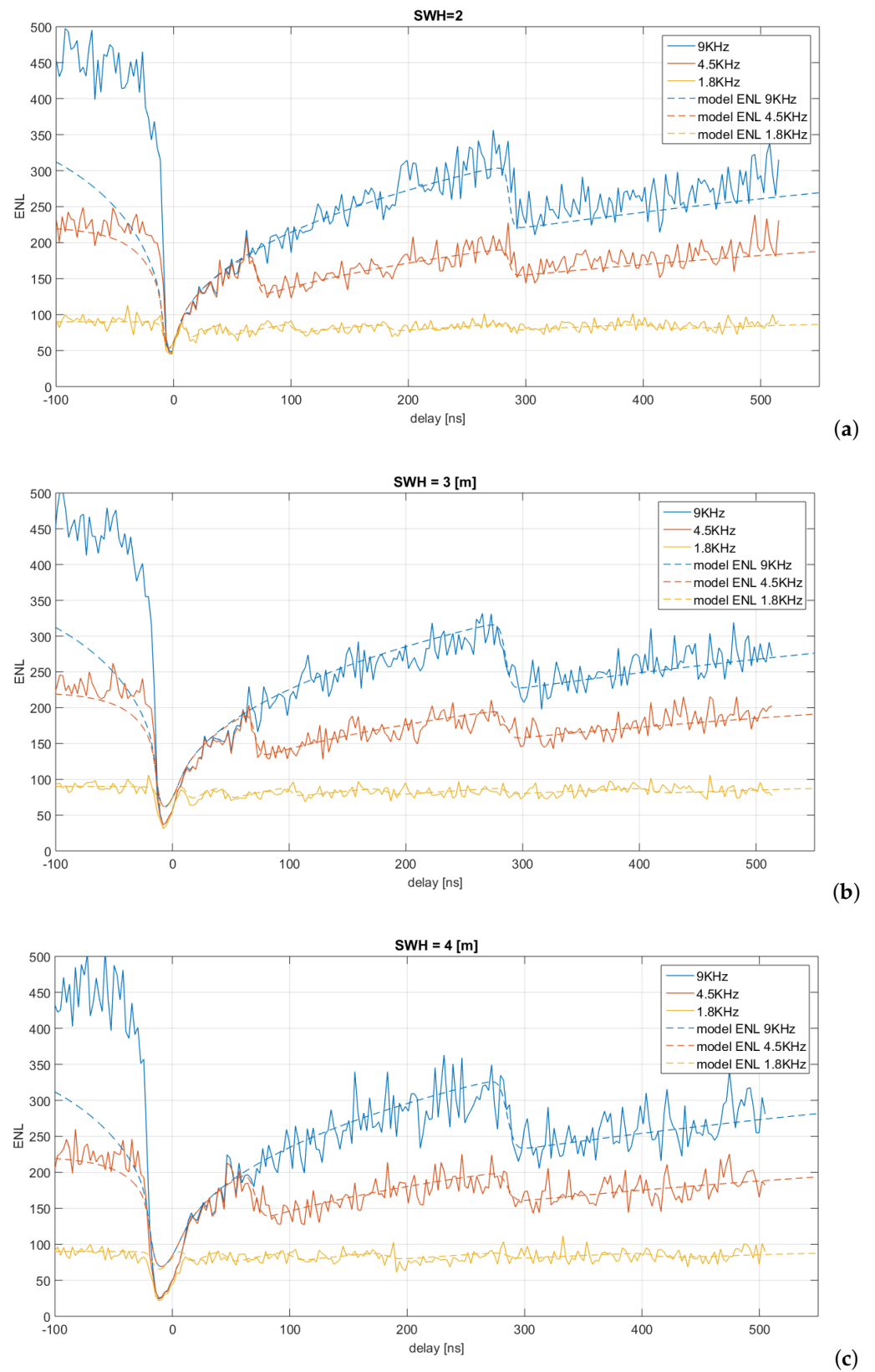


Figure 4. Cont.

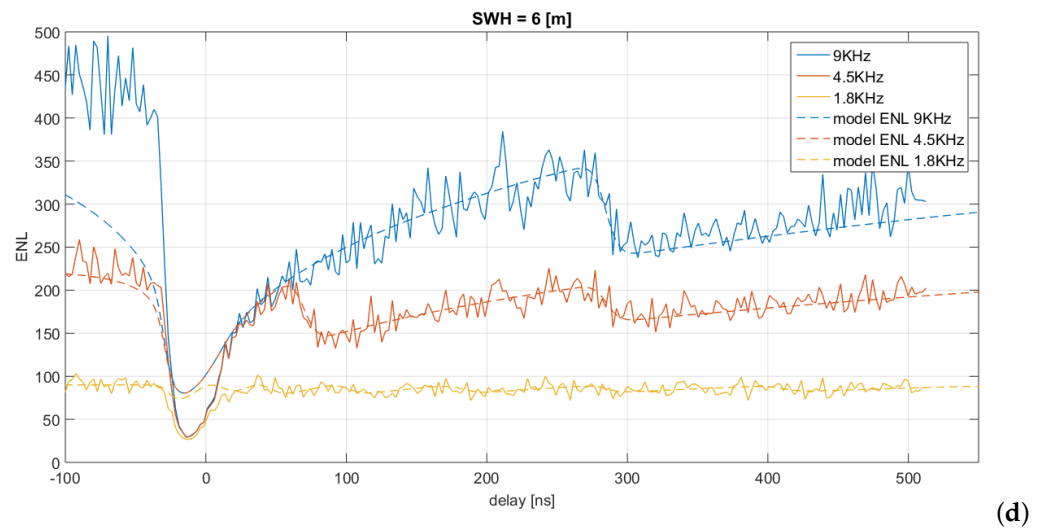


Figure 4. ENL values for different values of SWH, achieved using open ocean S6-MF data. Output posting rate is 20 Hz. ENL (solid-line) is plotted as a function of the delay time (in samples) and different factors (1,2,5); the corresponding theoretical trend is shown with dashed line. (a) $SWH = 2$ m; (b) $SWH = 3$ m; (c) $SWH = 4$ m; (d) $SWH = 6$ m.

4.3. Geophysical Parameters Estimation

The σ_0 , the sea surface height (SSH), and the significant wave height were retrieved from all the 256 S6-MF L1A pole-to-pole passes from cycle 9 and processed with the three different decimation factors considered in the previous section by making use of a geophysical retracker based on the model in [15].

Bias. It is known that the use of high PRF in acquisition introduces a bias in the estimate of the geophysical parameters [12,17]. Differently from that reported in the cited papers, this bias was evaluated using the original S6-MF PRF as reference and evaluating the difference in accuracy in case of a decimation equal to 2 and 5, the last corresponding to an acquisition of about 1.8 kHz. In Figure 5, the SSH, SWH, and σ_0 are reported. It is worth noticing that the estimated bias is on the order of few centimeters for SWH and below 0.4 cm for SSH. As expected, the bias is more pronounced with respect to the ≈ 1.8 kHz case (red lines) and slightly increases with the SWH. For σ_0 , the biases are below 10^{-3} dB and do not show a dependence on SWH.

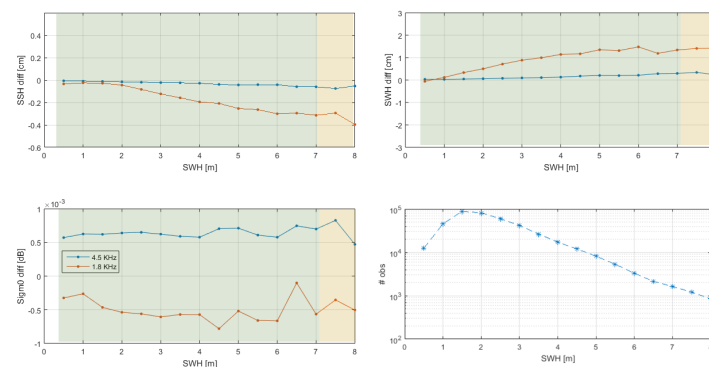
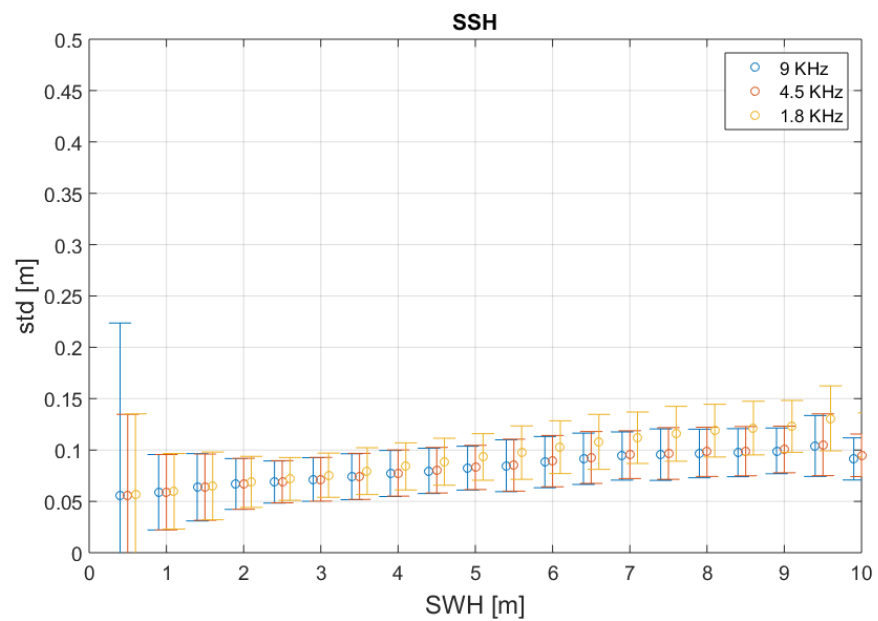


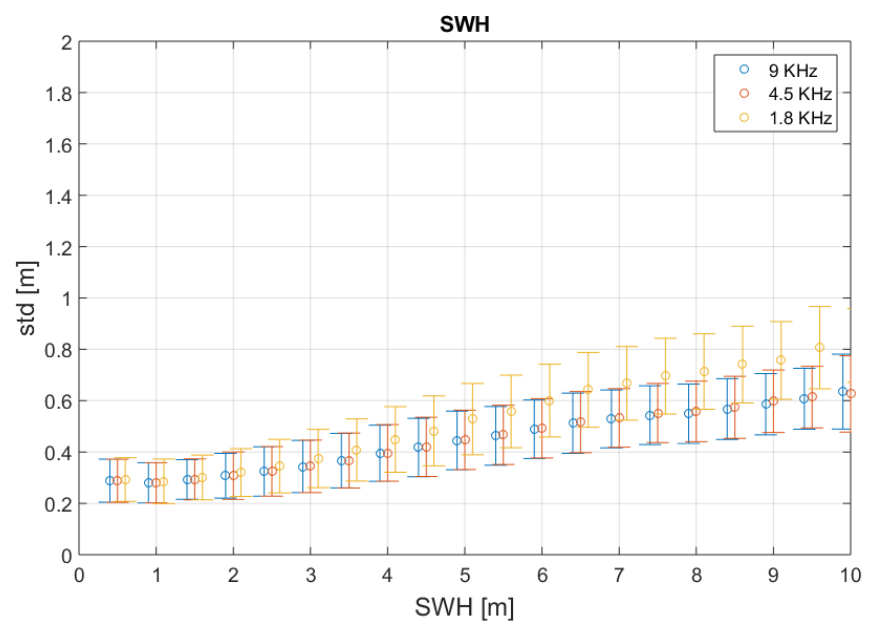
Figure 5. Bias of geophysical parameters achieved at two different decimation factors with respect to the original PRF, for S6-MF open ocean data, as a function of the SWH. Blue lines: bias between 9 kHz and 4.5 kHz (decimation factor 2); red lines: bias between 9 kHz and 1.8 kHz (decimation factor 5). Top left: SSH; top right: SWH; bottom left: σ_0 . The bottom right plot reports the number of available observations as a function of the SWH. The shaded green areas are where more than 2000 observations are available; in the orange areas, less than 2000 are available.

Precision. In Figure 6, the σ_0 , the SSH and the SWH precision (i.e., standard deviation) is shown as a function of the SWH. The dispersion of the sample standard deviation is addressed by the error bar around the estimated value, indicated by the circle and is a function of the number of observations. While the precision of σ_0 is basically unvaried with SWH, we see a decrease of the precision (i.e., the standard deviation increases) as SWH increases, for both SWH and SSH, regardless of the decimation factor used. This is addressed by the increasing trend of the circles with the SWH.

The partial correlation of the waveforms at high PRF has basically minimal or null effects on SWH and SSH precision, at least for low values of SWH. This means that the standard deviation is basically the same for low SWH, regardless of the decimation factor (represented by the different colors in Figure 6).



(a)



(b)

Figure 6. Cont.

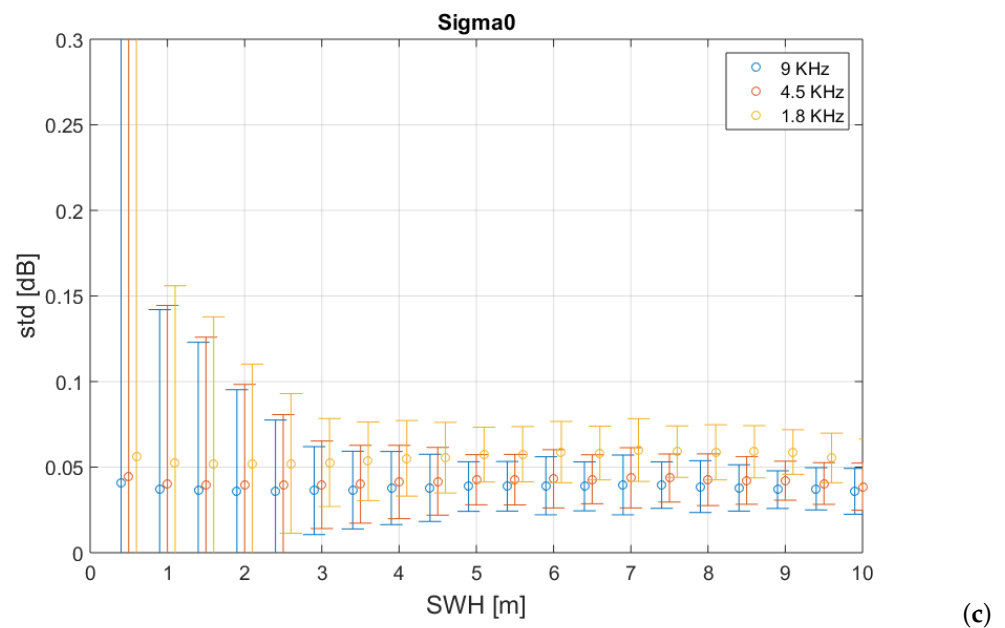


Figure 6. Geophysical parameters precision as a function of the *SWH* and for different decimation factor for the waveforms. (a) *SSH*; (b) *SWH*; (c) σ_0 . The circle indicates the estimated standard deviation while the error bar indicates the dispersion of the standard deviations.

5. Discussion

The autocorrelation function properties were widely explained in [12]. The behavior at the leading and trailing edges was interpreted in terms of waveform correlation (in the leading edge) and successive decorrelation (in the trailing edge), resorting to the van Cittert–Zernike theorem [18]. Here, the function was retrieved from real S6 data and for two different ocean conditions (*SWH*), with results in agreement with previous literature (compare Figures 3 and 4 with Figure 3 of [12]).

The observed decorrelation with the along-track distance with high *SWH* is expected: in fact, for higher *SWH*, portions of the sea surface contributing to the energy in the late-range bins are spread more broadly in the along-track distance. According to the van Cittert–Zernike theorem, this results in a broader Doppler bandwidth and in a faster decorrelation with along-track distance [12].

The theoretical ENL retrieved for increasing values of *SWH* shows that the leading edge is the most correlated part (ENL is low), and this is almost invariant with the *SWH*; instead, in the thermal noise area, the value is quite close to the maximum attainable (about 448 with S6-MF parameters, corresponding to the total number of pulses in a radar cycle that are averaged to generate a single LR pulse) since the thermal noise can be assimilated to a white noise, which decorrelates faster than the PRI interval.

This signal-free area is reduced, however, by the energy leakage from the leading edge of the waveform, resulting in a mixed area of thermal noise and physical signals with lower ENL values. The leaking is slightly different for different *SWH*, due to the shape of the leading edge, which is sharper for low *SWH* and blunter for high *SWH* [15]. This means that for high *SWH* more energy is leaked in the thermal noise area, and this reflects in a lower value of ENL in the mixed area as *SWH* increases.

The ENL was evaluated using different PRF, just by using different integer decimations of the waveforms. As expected, a higher sampling frequency provides a higher ENL (see Figure 4).

The high sampling frequency of acquisition has opened the possibility to obtain multilooked data at a posting rate higher than 20 Hz (typical of LRM products). This means we can obtain geophysical parameters at a higher rate with comparable accuracy with the ones in LRM products. Full-focusing processing becomes, then, fundamental to overcome

the LRM products for future missions such as CRISTAL. In a preliminary result, an open ocean dataset with $SWH = 2$ m was fully focusing processed and then multilooked at a posting rate of 140 Hz. The ENL profiles with the slant range are shown for different decimation factors in Figure 7. The trend of ENL with slant range is slightly different from the one achieved in the LRM case. A proper theoretical formulation and an in-depth analysis is then necessary in future work.

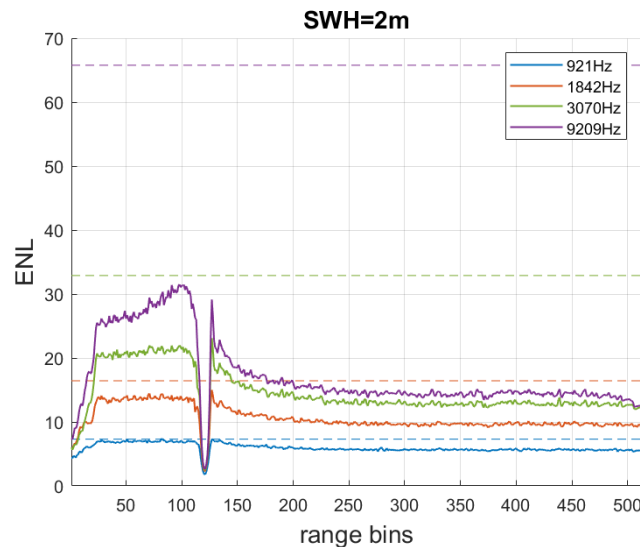


Figure 7. ENL (solid line) as a function of the slant range (x-axis) achieved from open ocean S6-MF data for $SWH = 2$ m and processed using FF processor. Different decimation factors are represented by different color codes; number of theoretical looks are shown with dashed lines.

6. Conclusions

In this paper, the theoretical and data-based autocorrelation function of the S6-MF pulse waveforms were investigated.

The ENL was evaluated from theory and compared with the same quantity estimated using open ocean datasets in different ocean conditions, showing a high degree of agreement. The ENL was estimated in different decimation cases with respect to the original S6 PRF. The plots confirmed that the high sampling rate acquisition system gains an equivalent number of looks. However, the partially correlated waveforms produce a bias with respect to the optimal sampling step, supposed at the Walsh bound.

It is important to point out here that the increase in the PRF improves the precision of the geophysical parameters, thanks to more looks available, but introduces estimation biases. These biases could be corrected empirically using a look-up table or more elegantly and properly handled by using a maximum likelihood estimator (MLE). This is crucial for the S6-MF mission, for having objectives to provide, such as reference mission and highly accurate time series of sea level measurements.

Author Contributions: Conceptualization: L.R. and P.G.; methodology: L.R. and P.G.; writing: L.R. and P.G.; review and editing: T.M.; supervision: C.D.; funding acquisition: C.D. All authors have read and agreed to the published version of the manuscript.

Funding: This study was funded by EU and ESA, under ESA Contract No. 4000134346/21/NL/AD.

Data Availability Statement: The raw data supporting the conclusions of this article will be made available by the authors on request.

Acknowledgments: This research was supported by an EU/ESA funded project named “Sentinel-6 Michael Freilich and Jason-3 tandem Flight Exploitation (S6-JTEX) study” under the supervision of Craig Donlon, and benefited greatly from altimeter data processing tools developed in Aresys.

Conflicts of Interest: Authors Lisa Recchia and Pietro Guccione are employed by the company Aresys. Author Thomas Moreau is employed by the company CLS. The remaining authors declare that the research was conducted in the absence of any commercial or financial relationships that could be construed as a potential conflict of interest.

References

1. Marghany, M. *Nonlinear Ocean Dynamics—Synthetic Aperture Rada*; Elsevier: London, UK, 2021.
2. Hammond, D.; Mennella, R.; Walsh, E. Short pulse radar used to measure sea surface wind speed and SWH. *IEEE Trans. Antennas Propag.* **1977**, *25*, 61–67. [[CrossRef](#)]
3. Raney, R. The delay/Doppler radar altimeter. *IEEE Trans. Geosci. Remote Sens.* **1998**, *36*, 1578–1588. [[CrossRef](#)]
4. Wingham, D.; Phalippou, L.; Mavrocordatos, C.; Wallis, D. The mean echo and echo cross product from a beamforming interferometric altimeter and their application to elevation measurement. *IEEE Trans. Geosci. Remote Sens.* **2004**, *42*, 2305–2323. [[CrossRef](#)]
5. Raney, R. A delay/Doppler radar altimeter for ice sheet monitoring. In Proceedings of the 1995 International Geoscience and Remote Sensing Symposium, IGARSS '95. Quantitative Remote Sensing for Science and Applications, Firenze, Italy, 10–14 July 1995; Volume 2, pp. 862–864. [[CrossRef](#)]
6. Zwally, H.J.; Giovinetto, M.B.; Li, J.; Cornejo, H.G.; Beckley, M.A.; Brenner, A.C.; Saba, J.L.; Yi, D. Mass changes of the Greenland and Antarctic ice sheets and shelves and contributions to sea-level rise: 1992–2002. *J. Glaciol.* **2005**, *51*, 509–527. [[CrossRef](#)]
7. Mugunthan, J.S.; Duguay, C.R.; Zakharova, E. Machine learning based classification of lake ice and open water from Sentinel-3 SAR altimetry waveforms. *Remote Sens. Environ.* **2023**, *299*, 113891. [[CrossRef](#)]
8. Goodman, J.W. *Statistical Properties of Laser Speckle Patterns*; Topics in Applied Physics; Springer: New York, NY, USA, 1963.
9. Raney, R.K. CryoSat SAR-Mode Looks Revisited. *IEEE Geosci. Remote Sens. Lett.* **2012**, *9*, 393–397. [[CrossRef](#)]
10. Walsh, E. Pulse-to-pulse correlation in satellite radar altimeters. *Radio Sci.* **1982**, *17*, 786–800. [[CrossRef](#)]
11. Scagliola, M.; Recchia, L.; Giudici, D.; Kuschnerus, M. Pulse limited waveforms from interleaved mode: An analysis on the achievable speckle noise reduction. In Proceedings of the OSTST Meeting, La Rochelle, France, 1–4 November 2016.
12. Egido, A.; Smith, W.H.F. Pulse-to-Pulse Correlation Effects in High PRF Low-Resolution Mode Altimeters. *IEEE Trans. Geosci. Remote Sens.* **2019**, *57*, 2610–2617. [[CrossRef](#)]
13. Donlon, C.; Cullen, R.; Giulicchi, L.; Vuilleumier, P.; Francis, C.; Kuschnerus, M.; Simpson, W.; Bouridah, A.; Caleno, M.; Bertoni, R.; et al. The Copernicus Sentinel-6 mission: Enhanced continuity of satellite sea level measurements from space. *Remote Sens. Environ.* **2021**, *258*, 112395. [[CrossRef](#)]
14. Egido, A.; Dinardo, S.; Ray, C. The case for increasing the posting rate in delay/Doppler altimeters. *Adv. Space Res.* **2021**, *68*, 930–936. [[CrossRef](#)]
15. Wingham, D.J.; Giles, K.A.; Galin, N.; Cullen, R.; Armitage, T.W.K.; Smith, W.H.F. A Semianalytical Model of the Synthetic Aperture, Interferometric Radar Altimeter Mean Echo, and Echo Cross-Product and Its Statistical Fluctuations. *IEEE Trans. Geosci. Remote Sens.* **2018**, *56*, 2539–2553. [[CrossRef](#)]
16. Recchia, L.; Scagliola, M.; Giudici, D.; Kuschnerus, M. An Accurate Semianalytical Waveform Model for Mispointed SAR Interferometric Altimeters. *IEEE Geosci. Remote Sens. Lett.* **2017**, *14*, 1537–1541. [[CrossRef](#)]
17. Dinardo, S.; Maraldi, C.; Cadier, E.; Rieu, P.; Aublanc, J.; Guerou, A.; Boy, F.; Moreau, T.; Picot, N.; Scharroo, R. Sentinel-6 MF Poseidon-4 radar altimeter: Main scientific results from S6PP LRM and UF-SAR chains in the first year of the mission. *Adv. Space Res.* **2024**, *73*, 337–375. [[CrossRef](#)]
18. Born, Max; Wolf, E. *Principles of Optics: Electromagnetic Theory of Propagation, Interference and Diffraction of Light*; Pergamon Press: London, UK, 1959.

Disclaimer/Publisher's Note: The statements, opinions and data contained in all publications are solely those of the individual author(s) and contributor(s) and not of MDPI and/or the editor(s). MDPI and/or the editor(s) disclaim responsibility for any injury to people or property resulting from any ideas, methods, instructions or products referred to in the content.